Strain Based Preload Measurement in Drive Axle Pinion Bearings

by

Anthony H. Thomas II

SUBMITTED TO THE DEPARTMENT OF MECHANICAL ENGINEERING IN PARTIAL
FULFILLMENT OF THE REQUIREMENTS FOR THE DEGREES OF

MASTER OF SCIENCE IN MECHANICAL ENGINEERING

and

BACHELOR OF SCIENCE IN MECHANICAL ENGINEERING
AT THE
MASSACHUSETTS INSTITUTE OF TECHNOLOGY

FEBRUARY 2005

Signature of Author...
Department of Mechanical Engineering
December 8, 2005

Certified by .........................................................................
Kamal Youcef-Toumi
Professor of Mechanical Engineering
Thesis Supervisor

Accepted by .........................................................................
Lallit Anand
Professor of Mechanical Engineering
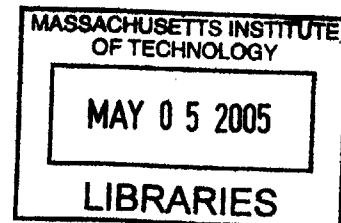
1

Strain Based Preload Measurement in Drive Axle Pinion Bearings

by

Anthony H. Thomas II


Submitted to the Department of Mechanical Engineering
on December 8, 2004 in Partial Fulfillment of the Requirements of the
Degrees of Master of Science in Mechanical Engineering and
Bachelor of Science in Mechanical Engineering


## ABSTRACT

Bearing setting has a significant impact on bearing life and system performance. A strain based load measurement technique that has been previously developed and patented will be used to measure preload in automotive drive axle pinion bearings. This technique utilizes strain gages placed in notches that have been machined into the outer diameter of a bearing cup. The performance of two gage types, semiconductor and metal foil, are compared. Preload in the pinion bearings is simulated in a machine by applying an axial load to a bearing assembly. The bearing assembly is rotated at various speeds and temperatures for each set of axial loads. Two notch geometries are compared for each set of tests conducted. An effort has been made to develop a finite element model that can be used to verify the results of the gage calibration. The results of the calibration reveal that metal foil and semiconductor gages can provide preload measurements that are accurate to within 3.7% and 7.7% of the full scale input load (73 lbs and 155 lbs) respectively.

Thesis Supervisor: Kamal Youcef-Toumi
Title: Professor of Mechanical Engineering

## Acknowledgements

First, I would like to thank my father Anthony, my mother Melinda, and my sister Michelle. They have always picked me up when I was down, and believed there was no limit to the things that I could accomplish in life. They provided me with the tools necessary to overcome the many obstacles that I have encountered throughout my undergraduate and graduate education at MIT. I thank my wife-to-be, Dwan Riddick, for being a source of stability and strength in my life. She has been my cheerleader when I have succeeded, and has consoled me when I have fallen short. She has always and will continue to bring out the best in me.

I want to thank my thesis advisors, Mircea Gradu and Professor Kamal Youcef-Toumi. Mircea has provided me with the resources and support necessary to complete my project work, as well as providing both academic and professional perspectives of the work I have done. Kamal had provided me with the help I needed to properly organize this work so that others can understand its implications.

I also want to thank the Timken Company and the many people here at Timken Research who helped make this work possible. I cannot name every single person who has had involvement in this project, but I would like to give a special thanks to James Nisly who was instrumental in the data acquisition, sensor design, and experimental testing aspects of the project. A special thanks also is given to the Driveline Group in Automotive Customer Engineering for their help and support throughout this process.

Last, and most importantly, I thank God for his many blessings. He has worked through me, allowing me to accomplish all that I do. "I can do everything through him who gives me strength." (Philippians 4:13)

3

# Table of Contents

# List of Figures

# List of Tables

# Nomenclature

| | |
|---|---|
| $\varepsilon$ | Strain |
| G | Gain |
| GF | Gage factor |
| $I_{excitation}$ | Excitation Current |
| MF1 | Metal foil gage in notch 1 |
| MF2 | Metal foil gage in notch 2 |
| Notch 1 | Shallow notch (geometry described in text) |
| Notch 2 | Deeper notch (geometry described in text) |
| $R_{gage}$ | Gage resistance |
| SC1 | Semiconductor gage in notch 1 |
| SC2 | Semiconductor gage in notch 2 |
| $V_{OUT}$ | Output voltage |
| $V_{IN}$ | Input voltage |

# Chapter 1   Introduction

Maintenance of bearing setting in a variety of applications can insure overall system robustness and efficient power transfer between assembly components, as well as reduce noise, vibration, and harshness.  Automotive drive axles are subjected to a myriad of loads and environmental conditions that present significant challenges when designing for such robustness and efficiency. During normal operation of the drive axle, the two pinion bearings must support the axial and radial loads transmitted trough the pinion shaft and withstand harsh environmental conditions. Tapered roller bearings have proven effective in supporting both the axial and radial loads, holding the pinion shaft in proper alignment with respect to the rest of the system, reducing friction, and improving overall system performance.

Loss of initial bearing setting can negatively impact bearing and system performance.  Setting (end play or preload) is defined as an internal loading in a bearing that is independent of any external radial and or axial loads.  Generally, in the case of a drive axle, preload on the pinion bearings must be maintained to insure efficient power transfer between axle gears.  If bearings are not properly set, accelerated gear wear and system vibration are likely to occur and adversely affect the life of the drive axle.  Much care must be taken to initially set bearings.  Regardless of how accurate the initial bearing setting is, it will tend to vary throughout the life of the bearing as a result of several factors including debris-induced wear and thermal and load induced deflections.  In order to monitor bearing preload, an effective method of preload measurement must be identified and characterized.  Without such a measurement system the amount preload variation in the drive axle remains unknown.

The technology that would allow for accurate measurement of pinion bearing preload throughout the life of an automotive drive axle exists and is readily available.  Devices have been developed specifically for this application, but their performance characteristics, particularly accuracy and resolution, have not been fully quantified for pinion bearings.  The technology described in US Patent 6,490,935 is of particular interest and relevance.   This technology describes the implementation of strain measurement sensors in one of the two bearing races in order to measure preload.   Such technology would allow for the monitoring of preload without disassembly of the drive axle.

The goal of this project is to identify and fully characterize the most appropriate preload measurement technique.  In Chapter 2 a brief overview of a generic automotive drive axle will be given.  Terminology relevant to the automotive drive axle will be introduced.  A description of the drive axle system and the tapered roller bearings contained in them is provided.  In Chapter 3 a selection of the most appropriate measurement method will be made.  This selection will be based upon the assessment of several technologies, and measurement techniques.  Previous measurement methods as well as proposed methods will be described.  In Chapter 4 the operation of the measurement sensors and their associated signal conditioning circuits will be described, as well as the experimental procedure that will be conducted to calibrate these sensors.  The accuracy and resolution of the measurement techniques will be quantified.  In Chapter 5 a finite element model will be presented.   The purpose of this model is to predict performance characteristics for various sensor configurations.  In Chapter 6 the experimental results will be presented and compared to the finite element model predictions.  The measurement technique

with the finest resolution, and greatest accuracy will be identified. If any discrepancy between the experimental results and the finite element model exists, an attempt will be made to describe reasons for the discrepancy. Finally in Chapter 7, conclusions will be drawn concerning the effectiveness and implications of this work, and suggestions for further work will be provided.

# Chapter 2  System Description

## 2.1  Automotive Drive Axle System Diagram

The term drive axle is often used to refer to the system including the mechanical components from the end of the drive shaft to the driven wheel end.  The primary purpose of a drive axle is to transfer the power produced by a vehicle's engine into useful torque at the wheel end.  Figure 2.1 provides an illustration of an automotive drive axle, and its location in a rear wheel drive vehicle.
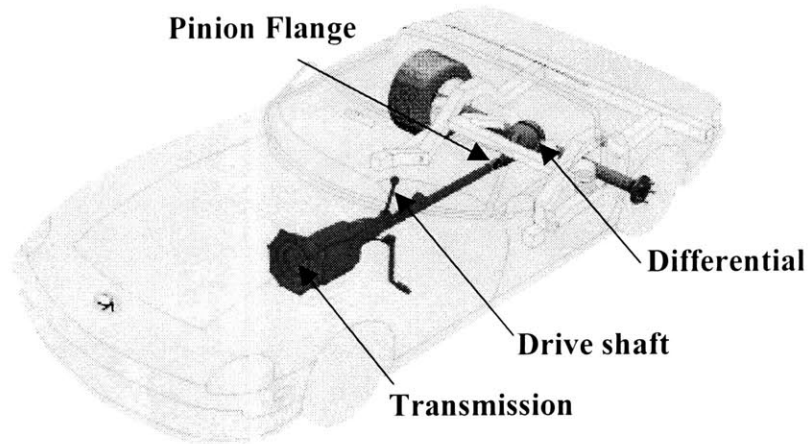


**Figure 2.1: Automotive drive axle in a rear wheel drive car (courtesy of http://www.autoshop-online.com/auto101/drive.html)**

Power from the drive shaft is transferred to the pinion shaft through a pinion flange.  The input pinion gear, which is mounted on the pinion shaft, meshes with the ring gear.  Power is then distributed to final drive axles, which are directly connected to the ring gear.  Figure 2.2 is an illustration of a hypoid pinion and ring gear arrangement.
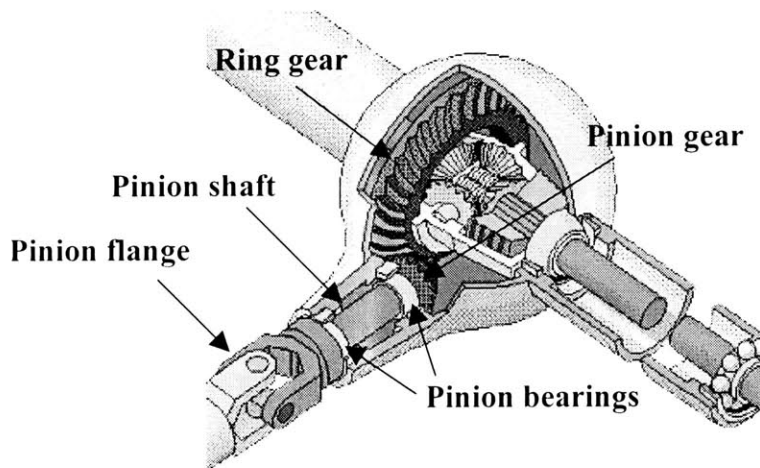


**Figure 2.2: Hypoid pinion in a drive axle (courtesy of http://www.autoshop-online.com/auto101/drive1.html)**

11

In this arrangement, as torque is applied to the pinion shaft via the pinion flange, the pinion gear attempts to climb up ring gear, pulling the ring gear down. Additionally, as the pinion gear rotates, it pushes itself away from the ring gear. Two pinion bearings mounted on the pinion shaft act to support these radial and axial loads. These bearings are dubbed the head and tail bearings. The head bearing is located closest to the pinion gear, and the tail bearing is located closest to the pinion flange. Tapered roller bearings provide the necessary support for the pinion shaft and its various loads. Figure 2.3 provides a closer view of a pinion shaft and its two tapered roller bearings.
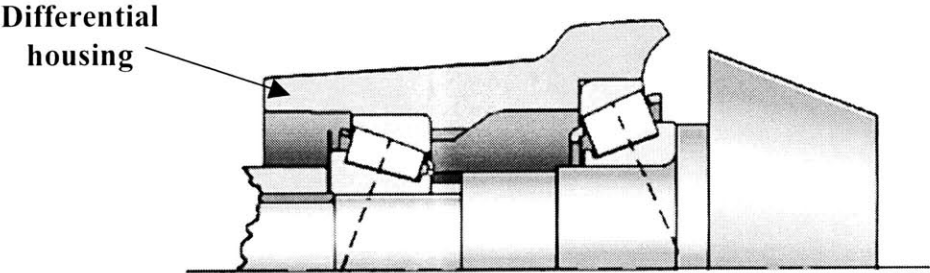


Figure 2.3: Pinion shaft and bearings (Courtesy of The Timken Company)

## 2.2 Tapered Roller Bearing Design

A tapered roller bearing is composed of a cup and cone, and a set of tapered cylindrical rolling elements. The rolling elements roll between the outer diameter surface of the cone and inner diameter surface of the cup. These surfaces are called bearing races. In most cases, one of these races is stationary. In the case of the drive axle, the outer race is generally stationary and fitted into the differential housing, while the inner race (cone) is pressed onto the pinion shaft. Figure 2.4 is a labeled cross section of a tapered roller bearing.
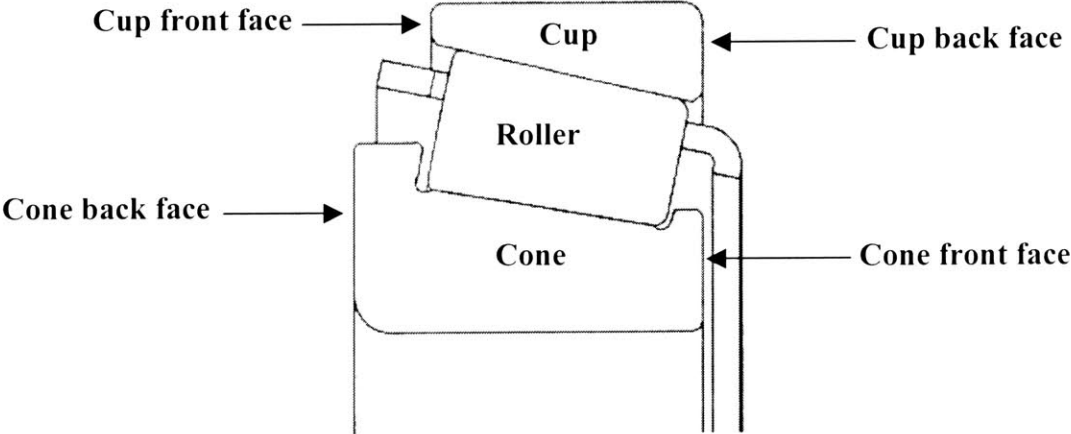


Figure 2.4: Tapered roller bearing cross section and its components (Courtesy of The Timken Company)

12

Line contact between the rolling elements and raceways of a tapered roller bearing help distribute load more evenly on each rolling element than a ball bearing does. This type of bearing is designed so that all the conical rolling elements' apices come together at a common apex. It is this characteristic that makes perfect rolling, which reduces the amount of friction generated in the bearing, possible. Figure 2.5 illustrates the typical geometry of a tapered roller bearing.
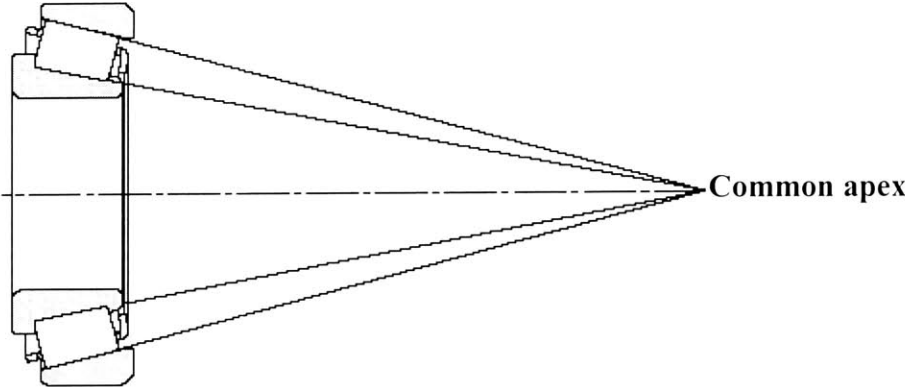


**Figure 2.5: Tapered roller bearing geometry (Courtesy of The Timken Company)**

Tapered roller bearings used in driveline applications are affected by a number of factors including load and speed, differential housing and pinion shaft stiffness, lubrication, bearing setting, thermal effects, and bearing design. Bearing setting refers to the specific amount of preload or endplay. End play is defined as "an axial clearance between rollers and races producing a measurable axial shaft movement when a small axial force is applied; first in one direction, then in the other, while oscillating or rotating the shaft", and preload is defined as "an axial interference between rollers and races such that there is no measurable axial shaft movement when a small axial force is applied in both directions, while oscillating or rotating the shaft"[1]. The absence of both endplay and preload in a bearing is called line-to-line. Bearing setting is achieved by moving one race axially relative to the other. This amount of displacement is a measure often used to quantify the amount of preload in a system. Figure 2.6 illustrates where this axial clearance is considered for bearing setting. Figure 2.7 shows the effect of setting on bearing life.
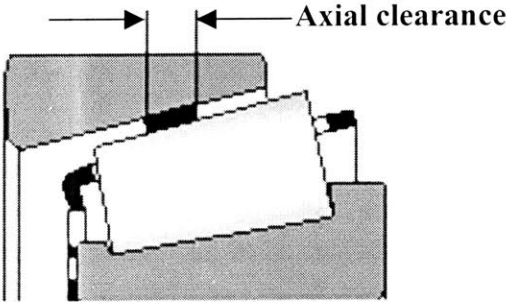


**Figure 2.6: Axial clearance that determines bearing preload (Courtesy of The Timken Company)**

---

[1] "Bearing setting techniques." Canton, OH: The Timken Company, 1985.
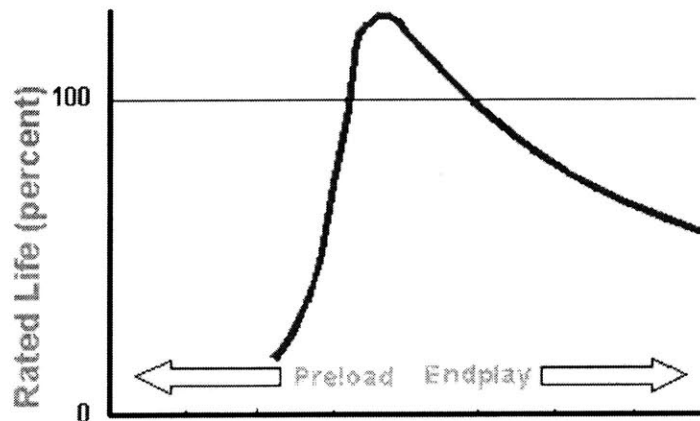
**Figure 2.7: Relationship between bearing life and setting (Courtesy of The Timken Company)**

## 2.3 Chapter summary

An automotive drive axle is a vital system whose function is to transfer power from a vehicle's engine to the drive wheels. A pinion shaft is one of the power transmission components in this system, and is subjected to both radial and axial loads. Tapered roller bearings support these loads and improve the overall performance of the pinion shaft and drive axle. Several factors must be considered when designing appropriate tapered roller bearings for drive axles, but of particular interest in this paper is the bearing setting. Proper setting in pinion bearings helps maximize bearing life, maintain proper gear mesh, and provide the appropriate system stiffness. Once the appropriate bearing preload has been selected and achieved, there must be a method to verify the maintenance of this preload. In the next chapter, various preload measurement techniques will be examined.

# Chapter 3  Preload Measurement Techniques

## 3.1  Overview of Bearing Preload

There are a few different ways to measure preload in a bearing. One method is called rolling torque measurement. Rolling torque is the amount of torque required to rotate a preloaded bearing. This method can be used both to apply initial preload, and monitor the preload of a bearing in service. Rolling torque measurements depend upon a number of bearing design factors. The magnitude of rolling torque in a preloaded bearing varies depending upon the bearing type, and a multitude of other operating conditions. The rolling torque method requires a bearing designer to select the appropriate correlations relating preload force to rolling torque.

The relative distances that the cup and cone back faces move during the bearing setting procedure quantify dimensional preload. Several dimensional preload methods exist, each using various gages to induce a specified displacement between the cup and cone back faces, projected onto reference surfaces. While application of bearing preload using this method is quite effective, measurement of preload in this manner is not feasible. The measurements required cannot be carried out because the cup and or the cone back faces are often inaccessible while the bearing is in service.

The final and most direct method of preload measurement is preload force. This method uses a direct measurement of the axial force required to compress the two bearing races together. There are a variety of gages and presses used to apply preload in this manner, but the measurement of preload force poses a challenge to designers.

## 3.2  Preload Force: Strain Based Measurement

Measurement of the preload force exerted on a bearing in service requires strain-based measurement devices situated in or on one of the bearing components (cup, cone, or roller). There are several ways to measure strain. In the following sections, several of these methods will be discussed. For each method, the following characteristics will be considered: operation, sensitivity, resolution, temperature effects, and advantages and disadvantages of the various techniques relative to each other.

### 3.2.1  Mechanical gages

The earliest strain measurement gages were mechanical strain gages. Initially screw micrometers were used to measure an overall change in length of a body under load. This was a crude strain measurement method, and only allowed for global measurements of strain; stress concentrations could not be identified with this technique.

As technology advanced, micrometer mechanical strain gages were made obsolete by extensometers. These gages measure the strain in bodies to which they are fixed through a system of levers. In the more advanced applications, light beams and mirrors are arranged to appropriately magnify the response. The highest resolution was achieved using the Huggenberger and Porter-Lipp type extensometer gage. These gages could measure strains as small as 10 $\mu\varepsilon$, using a magnification ratio of approximately 3000. The bandwidth of this measurement technique limits its usefulness to static strain measurement. Disadvantages of this

technique include its large bulky size; the minimum gage length is approximately ½ inch. The term gage length refers to the distance between the two attachment points of the extensometer. By modern standards, this gage length is very long.

### 3.2.2 Optical gages

An optical strain gage manipulates light beams to obtain strain measurements. One type of optical gage utilizes optical interference phenomena. Essentially this gage was an extensometer in which two optical plates are fastened to a substrate directly, or through a system of levers for strain amplification. The relative motion between the two optical flats would cause interference fringes to move past a reference point. The number of counted fringes translates to a strain measurement. This gage type is known as a Tuckerman gage. Maximum measurement bandwidths for this gage are approximately 150 Hertz. This gage type is extremely sensitive, has gage lengths of approximately ¼ inch, and the associated instrumentation for the gage is bulky in size.

### 3.2.3 Capacitive gages

A capacitive strain gage utilizes electrical capacitance to measure changes in length. Two metal conducting plates are mounted to a body, spaced a known amount, and separated by an insulator. Induced strains in the substrate cause a change in the measured capacitance. The biggest disadvantage of this technique is its undesirable sensitivity to vibration. Mounting and clamping these gages also pose significant challenges to a user.

### 3.2.4 Bonded resistance gages

A bonded resistance strain gage is composed of a foil or wire grid mounted on a paper or plastic substrate. This substrate is then bonded to the strained body. As the material is strained, the length, and thus the resistance of the gage change. To detect these small changes, the gage must be connected to an electric circuit. In one popular arrangement, the measurement gage, and three accompanying resistors in this electric circuit together are called a Wheatstone bridge. A potential source of error in a Wheatstone bridge is gage mismatch. Nominal values of resistance will vary between the four resistors in the bridge. Details describing the operation of Wheatstone bridges can be found in various texts, and does not need to be included here. It suffices to say that there are three configuration options for the Wheatstone bridge: quarter bridge, half bridge, and full bridge. Each bridge configuration utilizes a varying number (one to three) of "dummy" gages to help filter out thermal strains and temperature induced changes in resistance, which both interfere with the measurement of mechanical strain. The Wheatstone bridge also amplifies the output voltage resulting from the change in gage resistance.

Gage factor quantifies the gages sensitivity, and is defined as the ratio of the change in gage resistance divided by nominal gage resistance to unit strain. The gage factor for wire and foil gages is approximately 2. This gage factor varies with temperature. In addition to temperature induced gage factor variations, the thermal coefficients of expansion for the substrate and gage are often different, and often cause thermal strains. These effects resulting from temperature variation can be calibrated for through the proper use of the Wheatstone bridge and dummy gage, or through a series of calibration data points.

16

There are two types of bonded resistance gages: wire and foil. Wire gages have higher cross sensitivities than foil gages. Cross sensitivity is an effect resulting from sections of a gage grid perpendicular to the gage axis, or the axis of strain to be measured. The gage therefore is sensitive to strains normal to the gage axis. This is an undesirable effect when a body is subjected to strains in various directions and one wishes to isolate and measure only certain strains.

### 3.2.5 Piezoresistive

Piezoresistive gages also exhibit changes in resistance proportional to strain. These devices however require an external current source. The piezoresistive effect is not to be confused with piezoelectric effect. Piezoelectric devices exhibit a change in voltage proportional to strain. They require no external source of power, and only produce an output voltage for varying strains. Because they are constantly supplied with current, piezoresistive devices can measure both static and dynamic strains.

The sensitivity of piezoresistive strain gages is approximately 50 to 70 times that of bonded foil or wire resistance gages. Piezoresistive gages suffer from the same types of environmental effects as bonded resistance gages. Although they offer higher sensitivities, piezoresistive gages are more sensitive to temperature variations than bonded resistance gages. To make matters worse, the gage factor of piezoresistive gages often varies non-linearly with temperature, and presents an even greater calibration challenge that foil or wire gages do.

## 3.3 Proposed Preload Measurement Solutions

In order to measure bearing preload, bonded resistance and piezoresistive strain gages will be used. Both gages offer superior resolution and accuracy. These gages are also very small in size, and readily available. Neither of the gages is extremely expensive, and the same hardware and software can be used to calibrate, and collect test data from both gages. The piezoresistive gage is especially attractive because of its high gage factor, and potentially high accuracy measurement capability. The thermal instability problem associated with both gages will be mitigated by only using the gage at room temperature, and using signal conditioning hardware that will allow for the filtering of low frequency gage temperature variation. This eliminates the necessity of a full temperature calibration of the gage.

The gage factors for the metal foil and semiconductor gages are 3.25 and 155, respectively. Using the appropriate gain for each gage (metal foil gain set to 838.46, semiconductor gain set to 21.81) yields a strain output of 100 $\mu\varepsilon$/V (See Appendix A). The sensor bandwidth does not limit the performance of the either of the gages. All of the measurements are static. In the real-world application of these sensors in bearings, preload variation is not constantly monitored. Instead it is checked periodically since it does not vary from one rotation to the next. For this reason, the tests conducted involve the measurement of a load applied for a long period of time (approximately one minute).

These two methods require the installation of the gages on one of the bearing races. Since the outer race is stationary in the majority of pinion applications, strain gages will be installed in

17

notches machined on the outer diameter of the bearing cup[2]. By removing material from the outer race, a thin cross section beam element is created. This beam element bends as the bearing's rolling elements pass over the section. The strain levels, and therefore strain measurements, in the bearing are amplified as a result of the reduced cross sectional area of the bearing cup section in the notch. Shock and vibration are accounted for by averaging the values of strain measured by the gages for several rotations instead of simply taking the maximum strain value obtained from each roller pass. A further discussion of this strain measurement method can be found in the referenced literature. Figure 3.1 depicts this notch arrangement in the bearing.
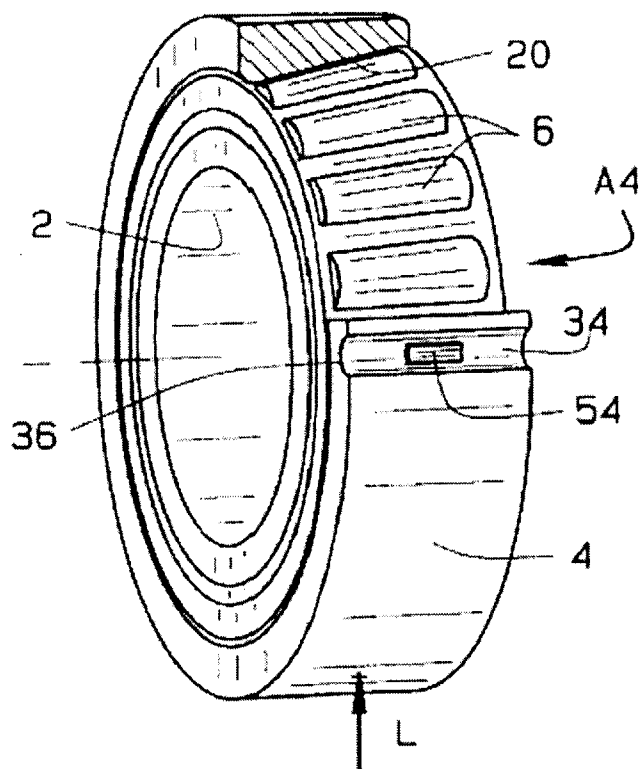


Figure 3.1: Bearing with machined notch for instrumentation of strain gage[2]

## 3.4 Chapter Summary

In the first section of this chapter, the three main bearing setting techniques were introduced. Each method was described, and its effectiveness as a preload measurement method evaluated. As a result of this evaluation, the most feasible preload measurement method, preload force, was selected. A non-exhaustive list of strain based measurement methods was presented. For each technology, an explanation of how it works was given. The potential advantages and disadvantages for each strain measurement technique were explained. As a result of this benchmarking effort, it was decided that for this particular application, piezoresistive and bonded strain gage technology were the most appropriate strain measurement sensors to determine

---

[2] US Patent number 6,490,935

18

bearing preload. Both gages are affordable, small in size, and provide excellent sensitivity and measurement resolution for preload measurement. In the next chapter, the operation of these two gage types will be described, and a method to quantify their measurement capabilities will be illustrated.

# Chapter 4  Experimental Apparatus and Procedure

## 4.1  Gage Measurement and Operation

Two strain gage types will be used to monitor bearing preload: foil and piezoresistive. Each of the gages will be installed into a notch on the bearing cup surface. In a preloaded bearing, each roller exerts both an axial and radial force on the cup raceway. The axial component of this roller load provides a measure of preload.

As rollers pass over the notched section of the cup, the reduced cross section beam created by the notch will be displaced radially. As a result of this displacement, the beam element will experience not only a radial strain, but also a circumferential strain. The strain gages are geometrically oriented to measure the circumferential, or hoop component of this strain. The width of the notch should be approximately the same as the roller diameter in order to measure the displacement caused by a single roller. In order to simplify the installation of the gage, the notch will have a flat surface instead of an arc shaped one. Figure 4.1 shows the notch geometry and its behavior under roller load.
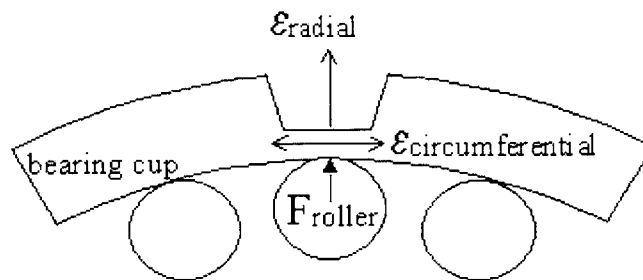


**Figure 4.1: Notched bearing cup and resulting strains under roller load**

## 4.2  Gage Performance and Signal Conditioning

Both the semiconductor and foil gages measure changes in resistance resulting from load-induced strains. The equations found in Appendix A describe how these measured changes in resistance, combined with the gage characteristics, are used to obtain strain values.

The signal-conditioning configuration selected for this preload sensing bearing is a constant current strain gage bridge. In this configuration the gage will be supplied with a constant current, and the strains induced by roller passes can be measured. AC coupling the data recorder to the gage filters out low frequency noise resulting from temperature variations of the gage and lead wires. Once this low frequency noise is filtered out, the signal is amplified, and then sent through a low pass filter. This final filter removes high frequency noise, primarily electromagnetic interference, and radio frequency interference. The signal is then sent to the analog to digital converter then to the PC for final digital manipulation and output.
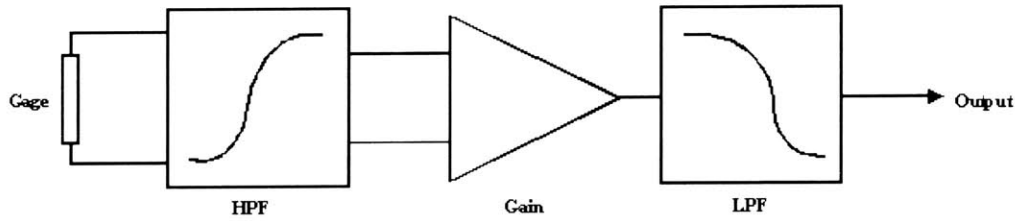
Figure 4.2: Constant current strain gage conditioning

## 4.3  Procedure

Four notches were machined into a single bearing cup. Two different notch depths were selected for the tests. The reason for having a shallow and deep notch was to determine whether or not the strain amplification from a shallower notch would be sufficient in obtaining preload measurements. The shallow notch geometry selected was the minimum amount of space required to comfortably fit the strain gage, temperature sensor, and its wire leads without extending beyond the cup outer diameter. The cup would have to be pressed into the tooling for the test machine, and in the real world application, the cup is pressed into a differential housing. The sensor and its associated hardware must therefore fit within the envelope of the cup outer diameter. The deep notch was simply twice as deep as the shallow notch. In two notches (one of each depth) foil gages were installed. In the other two notches (one of each depth) semiconductor gages were installed. Along with both sets of gages, temperature sensors were included to allow for the measurement and correction of temperature induced gage variations. Figure 4.3 shows the bearing cup notches after the installation of the gages and temperature sensors.
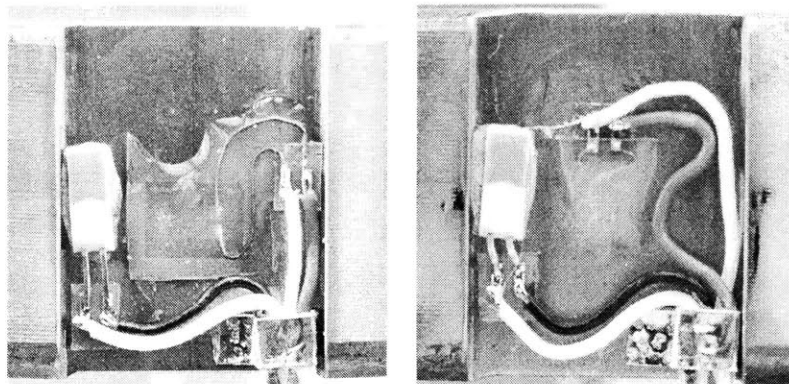


Figure 4.3: Foil gage (left) and semiconductor gage (right) fitted into cup notch

After the strain gages and temperature sensors were installed, the notches were covered with a protective epoxy.

The gages were then connected to a current source, and calibrated. This initial calibration was conducted to insure proper gage installation and operation. The actual test procedure was conducted in a load cell called the Torque Tester. This machine simulates the axial loading of a preloaded bearing. The bearing cup is pressed into a stationary tooling fixture, which simulates the differential housing. The cone is then brought into contact with and rotated in the cup.

21

Preload is simulated by pressing the cone into the cup. A circulating oil flow through the tooling and a heat exchanger are used together to maintain a fairly constant bearing temperature so that gage factor variation as a result of temperature drift is minimized. Figure 4.4 shows the test setup in the Torque Test machine.



Hydraulic press to actuate axial load

Tooling containing the bearing cup

Strain gage wire leads

Temperature controlled oil flow
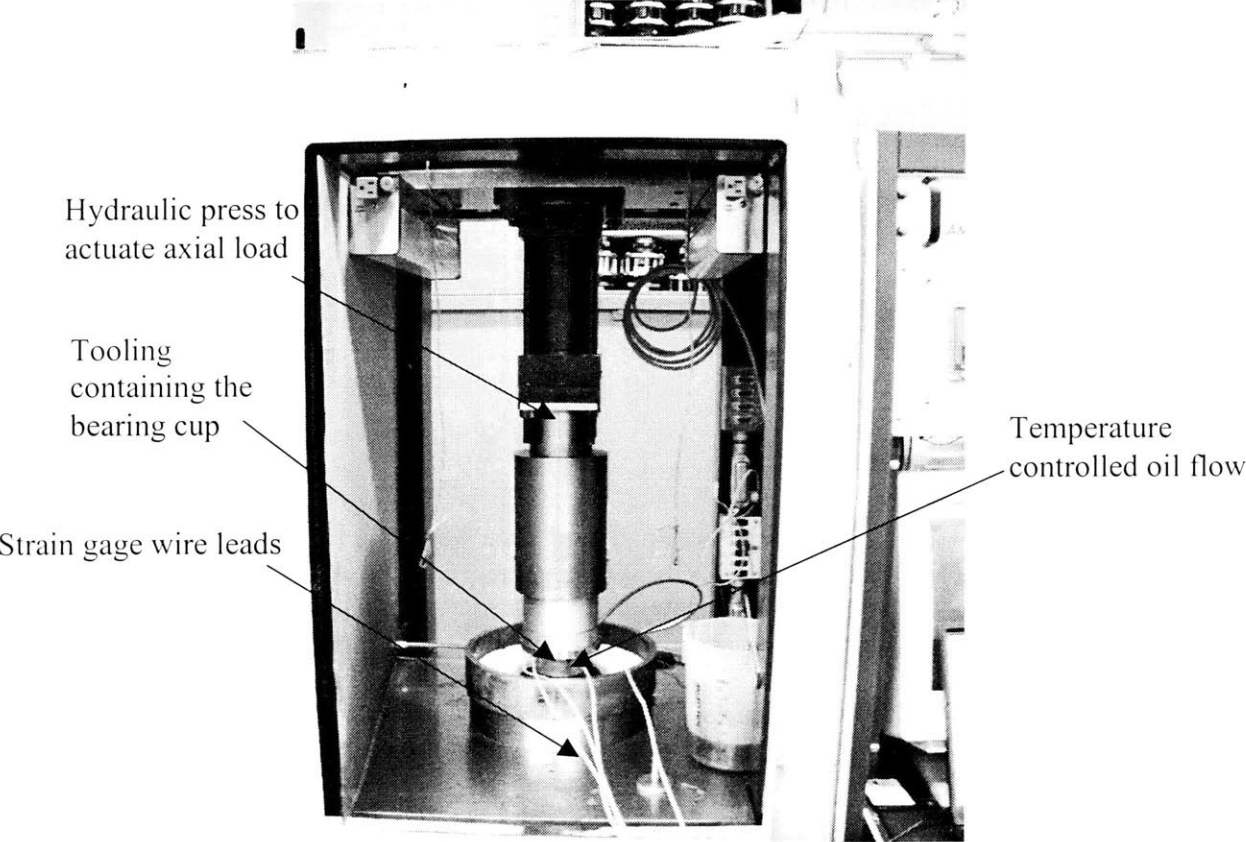
**Figure 4.4: Torque Tester**

The circumferential component of notch strain is measured by the gages. A calibration curve is constructed in which notch strains are measured and recorded for various controlled axial loads applied to a rotating bearing. Table 4.1 summarizes the test matrix of various load and speed inputs used to test the gages.

| Speed (rpm) | Load 1 (lbs) | Load 2 (lbs) | Load 3 (lbs) | Load 4 (lbs) |
|---|---|---|---|---|
| 800 | 500 | 1000 | 1500 | 2000 |
| 1000 | 500 | 1000 | 1500 | 2000 |
| 1200 | 500 | 1000 | 1500 | 2000 |

**Table 4.1: Test matrix for load cell test rig**

For each test conducted, a rotational speed was maintained, and successively increasing axial loads were applied to the bearing. Each load increment indicated in Table 4.1 was held constant for one minute before sequencing to the next load. The loading and unloading sequence was

22

repeated five times to quantify sensor hysteresis. This entire test matrix was conducted at two temperatures: 100 °F and 150 °F.

## 4.4   Chapter Summary

The operation of the strain gages and their associated signal conditioning circuits have been briefly described. A test procedure has been introduced, and a method to determine bearing preload has also been set forth. The test procedure developed is intended to create a data set that correlates bearing notch circumferential strain to bearing preload. In the following section, the development of a finite element model will be described. This model will be used to verify the calibration results obtained from the experimental results.

# Chapter 5   Finite Element Analysis

## 5.1   Model Description

The main objective of the finite element model was to estimate the magnitude of strains at various locations in the notch resulting from bearing preload. Two notch geometries were analyzed, and are described by the hand sketches shown in Figure 5.1 and Figure 5.2. As was described in 4.3 the notch geometry was selected by determining the depth required for the sensor and wire leads to fit within the bearing cup outer diameter. From this section forth, the names notch 1 and notch 2 will be used to distinguish between these two notch geometries.
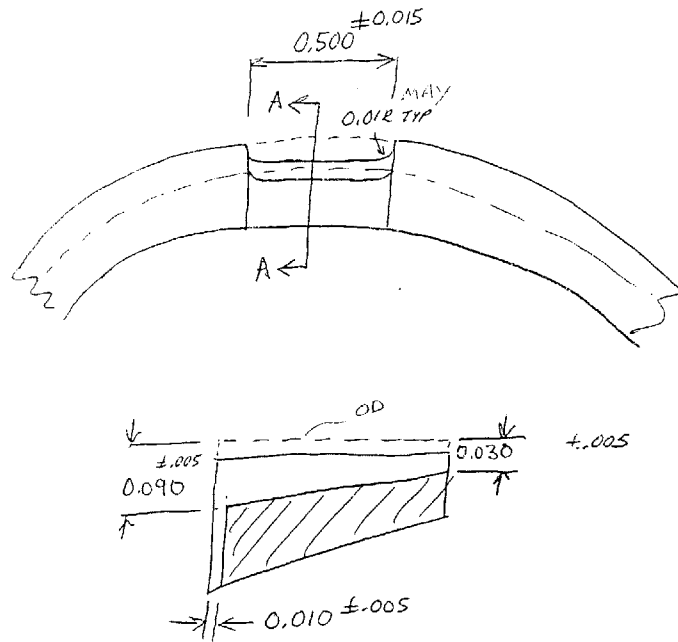


Figure 5.1: Notch geometry for notch 1

24
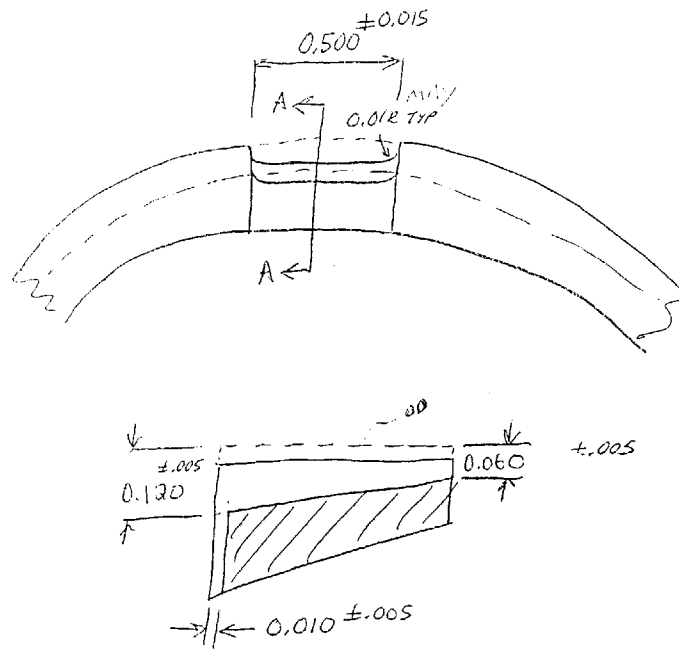
**Figure 5.2: Notch geometry for notch 2**

The original cup geometry was taken from a product database, and modified with the notches shown above. These bearing cups were modeled using 20 node quadratic brick elements. These were selected for their accuracy under bending loads.

The rollers were modeled using nonlinear uniaxial spring elements. The roller spring stiffness was calculated using a proprietary Fortran based module developed by The Timken Company. This module is configured to assume springs are connected to linear brick elements. The spring stiffness for each roller was modified to connect to the quadratic brick elements of this model. Springs connected to nodes located at the roller end edge of the brick elements were modified to be 1/6 the stiffness of springs connected to nodes in the interior of the roller area. This maintained uniform stiffness across the roller area at the quadratic element interface. The total stiffness of the spring elements modeling each roller was then proportioned to keep the total roller stiffness equivalent to the total roller stiffness calculated by the module. The stiffness of each of the springs at the symmetry plane was half that of springs located at interior nodes of the model. The cones and shafts were modeled using beam elements with a diameter equal to the cone mean diameter. It was assumed that the shaft was solid.
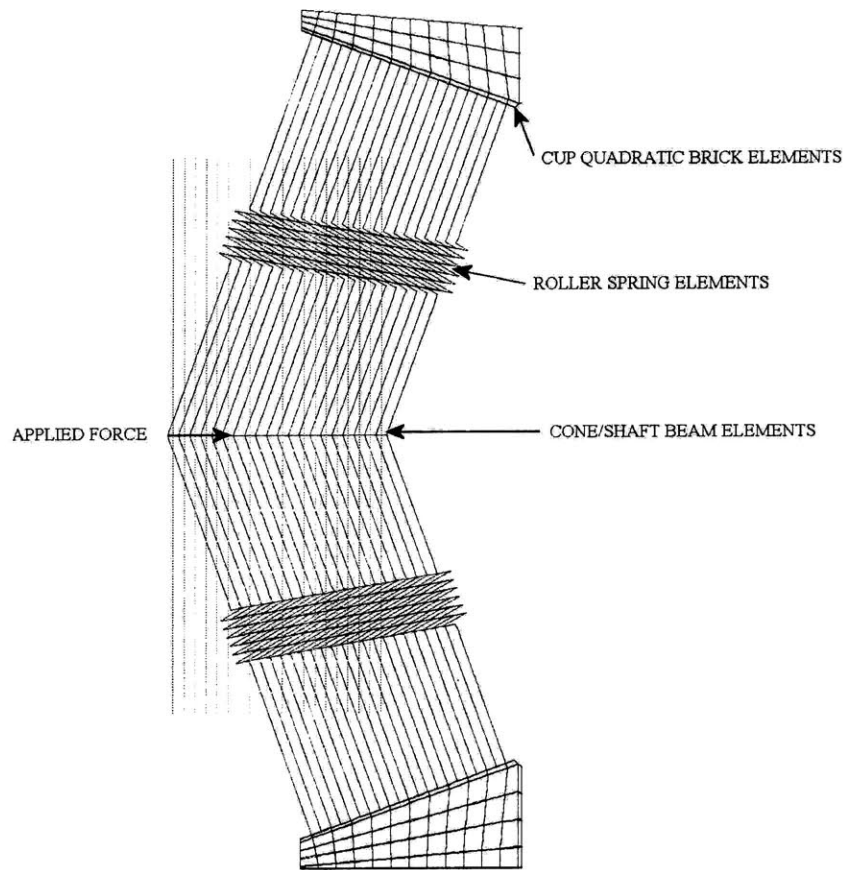
**Figure 5.3: Finite element model schematic**

This model is an approximate representation of a bearing under preload. A more accurate representation would take into account some subtle design characteristics of an actual tapered roller bearing. The roller and race are not in perfect line contact. The roller has a specific geometry characterized by various radii to adjust the stress distribution along the raceway. Additionally, the bearing cone often has an undercut to reduce stress concentrations that would normally exist at the roller end-cone contact point. As a result of these design details, the stress distribution in a tapered roller bearing is more complex than an equal stress distribution along the cup raceway.
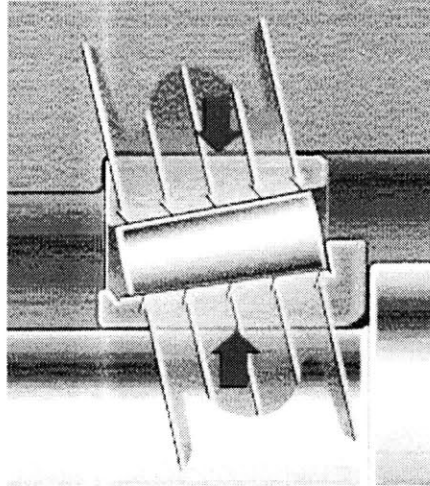
**Figure 5.4: Stress distribution of a standard roller under heavy load (Courtesy of The Timken Company)**

Bearing preload results from an axial displacement of the two races relative to one and other that is induced by applying a force to one race, and holding the other race stationery. Figure 5.5 below illustrates the loads applied to a bearing under preload, and the resulting forces exerted on the cup inner diameter by the rollers. Here, $F_{roller}$ is the force resulting from the roller spring stiffness, and $F_{preload}$ is the applied axial force in Figure 5.3.
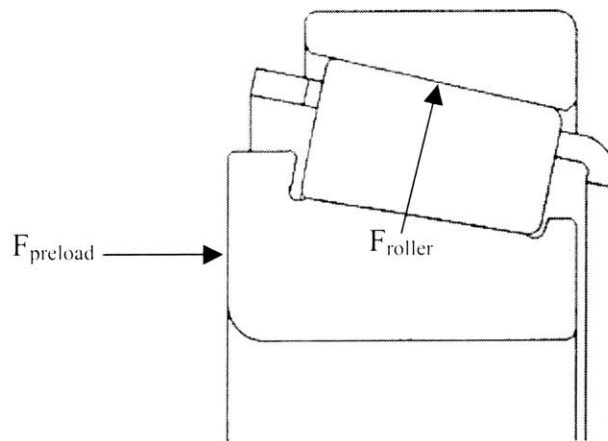


**Figure 5.5: Bearing under preload and the resulting reaction forces (Courtesy of The Timken Company)**

A 2000 lb axial load was specified, but because of the symmetry of the model, a 1000 lb load was applied to a half section of the cup at the end node of the beam sections. Nodes at the symmetry plane were constrained to remain normal to that plane. The cup back face nodes were constrained in the axial direction. These conditions resemble the behavior of a bearing cup pressed into an automotive drive axle differential housing.

## 5.2    Analysis Results

The finite element model predicts circumferential strains ranging from approximately 400 to 700 µε along the centerline of the notches.  As was expected, the deeper notch yielded strains higher in magnitude than the shallower notch.  Figure 5.6 is a graph plotting strain along the centerline of the notch versus the distance from the cup front face.  Figure 5.7 and Figure 5.8 are graphical plots of strain in the finite element model.  These images are best viewed using a full color display.  The loading condition for this data was a simulated 2000 lb preload.

**Strain Values at Notch Centerline**
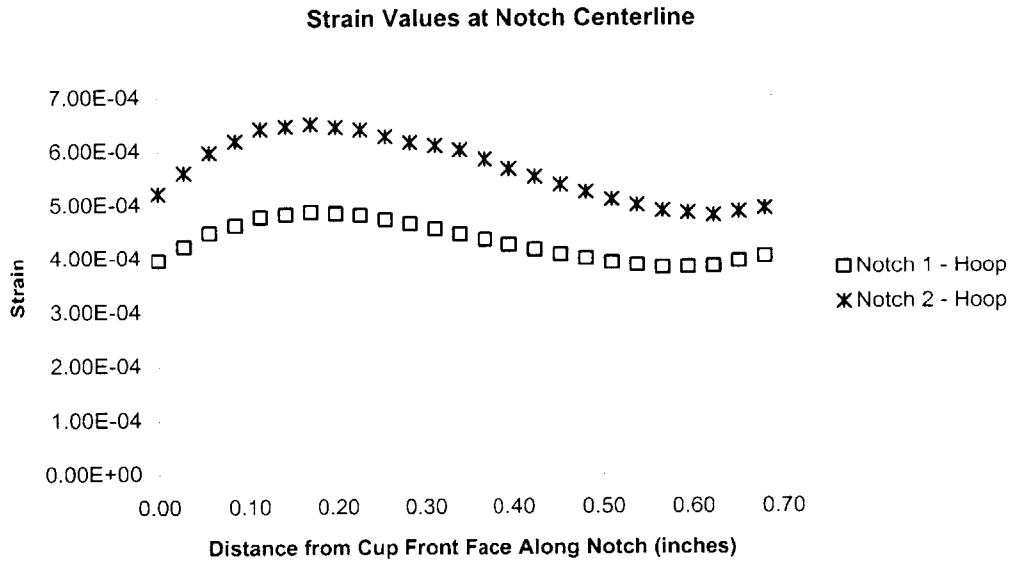


Figure 5.6: Strain values along notch centerline from cup front face to back face
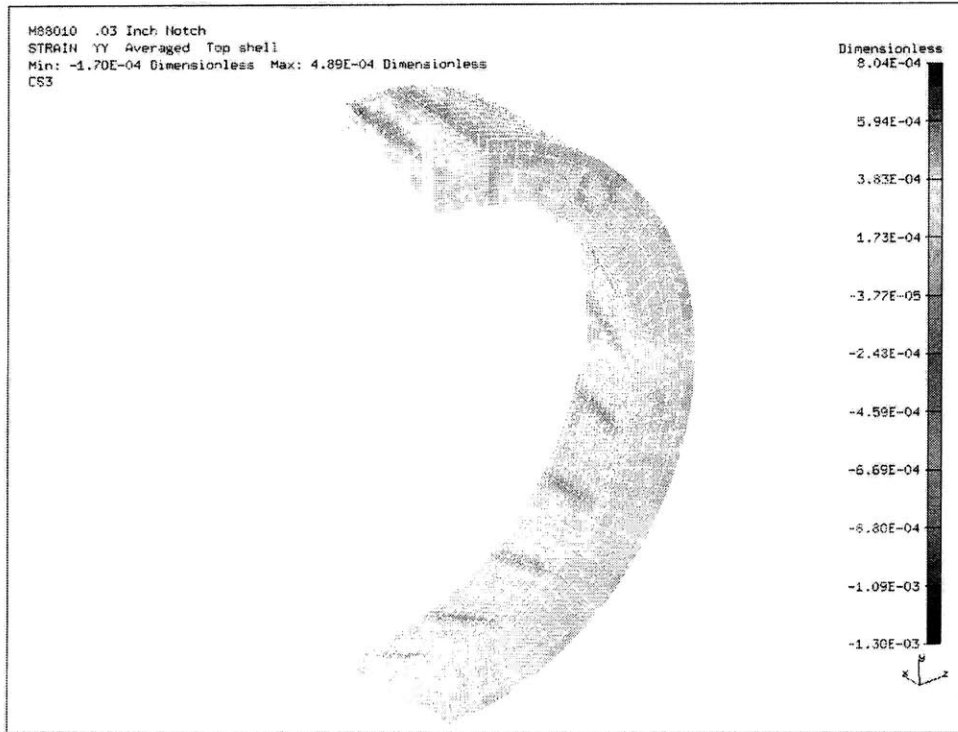
**Figure 5.7: Notch 1 finite element strain plot**
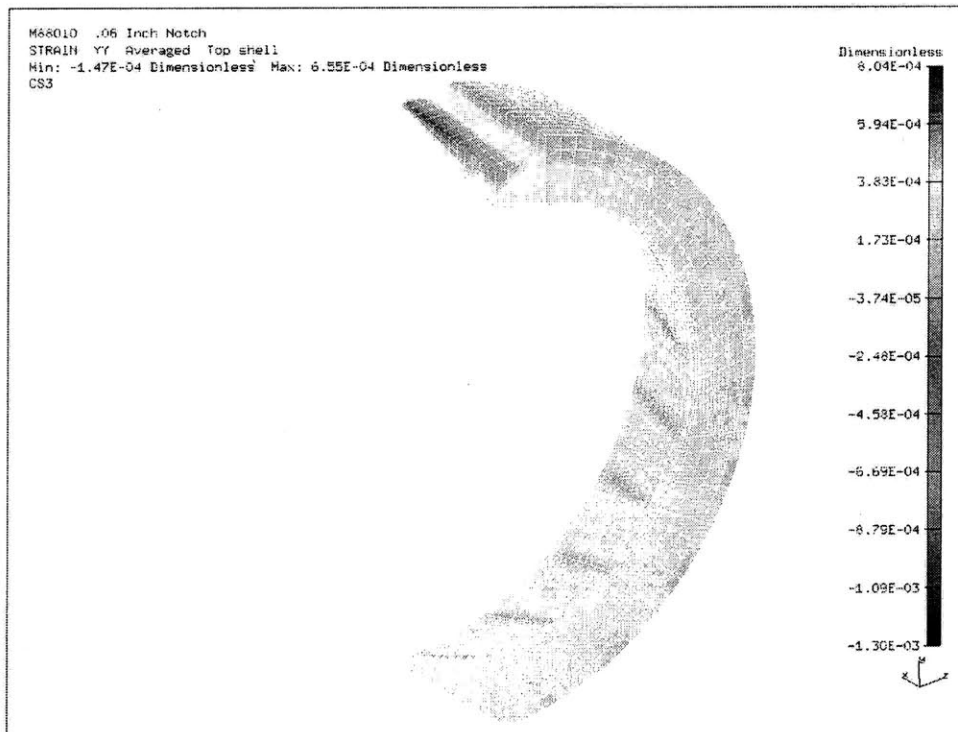


**Figure 5.8: Notch 2 finite element strain plot**

## 5.3 Chapter Summary

A finite element analysis has been completed in order to predict strain levels that will be measured by strain gages. The assumptions, boundary conditions, and loading conditions used were presented, and justified as appropriate for the simulation of preload forces on a bearing cup in a differential housing. In the next chapter, the results of the experimental tests will be presented and compared to the predictions made by this finite element model.

# Chapter 6   Experimental Results and Discussion

## 6.1   Test Results

Several parameters were varied in order to characterize preload measurement performance. These factors included temperature, speed, gage type, and notch geometry. Although the measurement characteristics vary with each of these factors, speed and temperature are of most interest and importance; in a real-world application gage type and notch geometry will be specified, held constant, and should remain known throughout the life of the measurement system. The results presented here will take this into account. Gage performance variations resulting from changes in gage type and notch geometry will be briefly discussed, but the focus of this section will be on gage performance variations resulting from changes in speed and temperature.

### 6.1.1   Gage Linearity

Gage theory for both the semiconductor and metal foil gages propose that the relationship between gage resistance and strain is linear (see Appendix A). It was assumed that the relationship between applied load and measured strain was also linear. This however may not be the case. The irregularities resulting from the bearing cup geometry and notches could lead to a non-linear relationship between strain and preload force. Another factor potentially contributing to a non-linear response is the unknown effect of the bonding between the strain gages and substrate.

Upon examination of the data, it was assumed that the relationship between measured strain and input preload force was linear. The degree of linearity, however, varies between the two gage types and notch geometries. To conduct a consistent analysis of the data, a linear relationship between preload force and measured strain was assumed. It is important to note, however, that linearity is not a necessary condition for proper gage performance. In its actual use, each gage would be individually calibrated. For each of these individual calibrations, repeatability is of most importance: the user is most concerned with being able to replicate any given calibration curve when collecting preload force data. Higher order relations could be used to fit the data to calibration curves.

To quantify the repeatability of the data, linear functions relating input preload force to measured notch strain were fit to each data set. Utilizing this linear relation, measured strain was used to back-calculate the applied preload. The calculated preload input values were compared to the measured preload input values. From this comparison, percent error, minimum and maximum absolute error, measurement certainty, and error percentage of full scale were determined. Measurement certainty is a single value that describes the tolerance of the measurement. For example, if the certainty of a measurement were ten units, this would mean that the measured value was correct to within ten units. Error percentage of full scale is the ratio of the certainty to the full range of possible outputs (in this case, preload force). It is important to note that no effort was made to do offset adjustment since the development of a global relation to fit multiple data sets was not needed.

31

In the following sections, gage performance will be presented. The preload measurement capabilities of each sensor will be quantified. Test measurements at various speeds, loads, temperatures, and notch depths will be compared. Sensor performance and its dependence on speed and temperature will be explored. The plots that will be displayed are a result of the test procedure described in Section 4.3. Each data set consists of five sequentially repeated loading and unloading cycles. Unless otherwise noted, additional data plots can be found in Appendix C.

## 6.1.2 *Metal Foil vs. Semiconductor*

The metal foil and semiconductor gages do not measure similar strain levels. The metal foil gage output was consistently approximately twice that of the semiconductor gage.

Figure 6.1 compares the output of one of the semiconductor gages to the output of one of the metal foil gages at 800 rpm and 100 °F in notch 1.
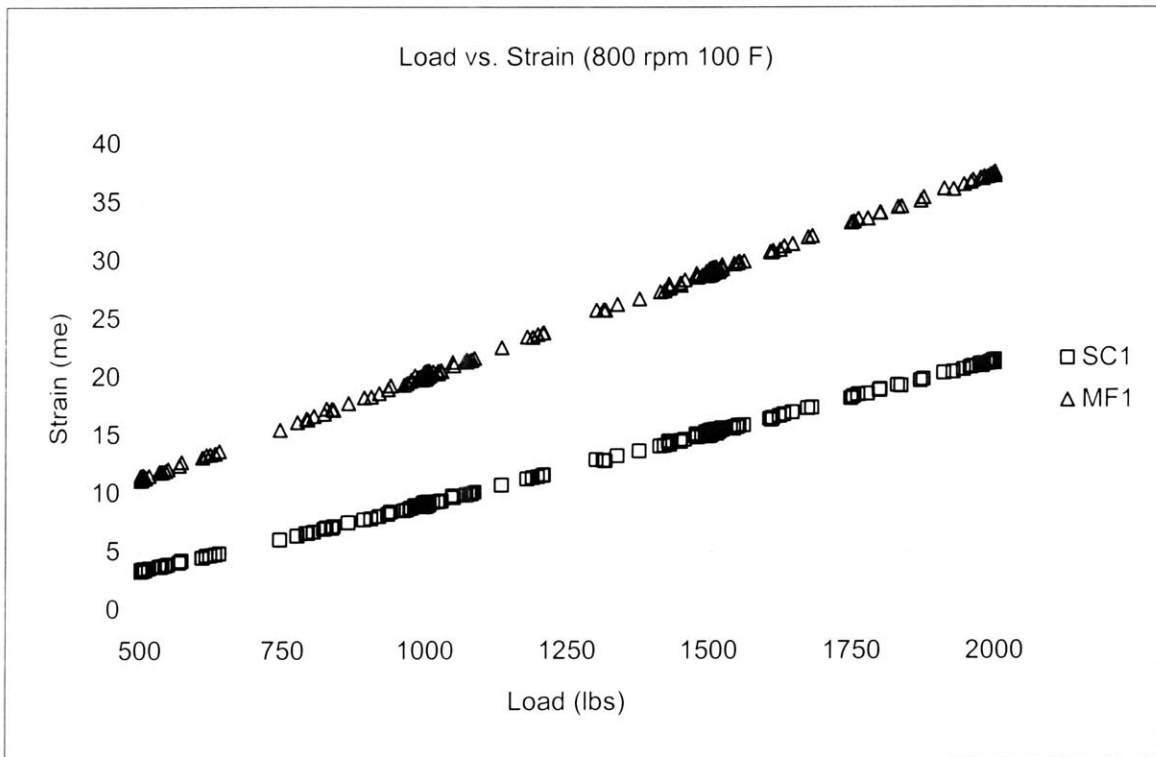


**Figure 6.1: Metal foil and semiconductor gage output comparison**

There are a couple of potential reasons why the output for the two gage types is so different. First, the resistance of the semiconductor gage provided by the manufacturer is a nominal value. The actual measured values of semiconductor gages one and two (labeled SC1 and SC2 in the data plots) were 13.9% and 11.5% below the nominal value of 350 Ω, respectively. Since nominal values of the semiconductor strain gage resistance were used to calculate measured strain, the plotted values are underestimates of the actual strain. Also, the bonding of the gage to the substrate may vary from one installation to another, as well as from one gage type to another. The effect that this has on strain values measured cannot be quantified.

## 6.1.3 Speed and Temperature Variation

Neither speed, nor temperature had a detectable effect on gage performance. Tests were conducted at three speeds (800, 1000, and 1200 rpm) and two temperatures (100 °F and 150 °F). At each of the speeds, gage output was extremely consistent. The speeds at which the tests were conducted were selected because they were deemed sufficiently far from the cut-off frequencies of both the low- and high-pass AC filters described in 4.2. Table 6.1 and Table 6.2 illustrate the consistency of gage performance with variations in speed and temperature, respectively. Both datasets are for the same gage in the same notch.

| SC1 | 100 F | | | | y=mx+b | |
|---|---|---|---|---|---|---|
| | Max error | Certainty | error % of full scale | Avg Temp (F) | M | b |
| 800 rpm | 4.69% | 51.57 | 2.58% | 99.7 | 0.0121 | -2.8229 |
| 1000 rpm | 6.51% | 64.48 | 3.17% | 99.8 | 0.012 | -2.4907 |
| 1200 rpm | 6.95% | 57.16 | 2.86% | 101.1 | 0.0119 | -2.7831 |

Table 6.1: Test results for semiconductor gage in notch 1 at 100 °F

| SC1 | 800 rpm | | | | Y=mx+b | |
|---|---|---|---|---|---|---|
| | Max error | Certainty | error % of full scale | Avg Temp (F) | m | b |
| 100 F | 4.69% | 51.57 | 2.85% | 99.7 | 0.0121 | -2.8229 |
| 150 F | 7.13% | 56.63 | 2.83% | 143.6 | 0.012 | -2.9447 |

Table 6.2: Test results for semiconductor gage in notch 1 at 800 rpm

## 6.1.4 Finite Element Results

The finite element model constructed to predict notch strains severely overestimates the actual measured strains in the bearing. The model constructed did not take into account the dynamic behavior of the measurement setup. In the test setup, dynamic roller passes induced strains in the bearing cup. In the finite element model, a static loaded roller was used to induce a strain on the bearing cup. Each cup modeled only contained a single notch, whereas in the tests conducted, the bearing cup contained four notches. The bearing cup in the experimental tests was press-fit into the housing of the tooling for the Torque Test machine. In the model, however, no press-fit was simulated. Instead the outer diameter of the bearing cup was simply supported. By refining the model, and accounting for these inconsistencies, a more accurate prediction of preload induced strains on the bearing cup may be obtained. One of the greatest challenges in predicting these strains using a finite element model is the variation of the behavior between the strain gage and the substrate resulting from the bonding procedure used to install the gages. Unfortunately, this variation cannot be easily quantified because of the variation introduced by human error.

## 6.2 Discussion

Notch depth has a significant effect on the strain response of the bearing cup, and therefore the gage measurement performance. According to the data averages, the shallower notch provides more accurate measurements than the deeper notch geometry. The amplified response obtained

from measurements in the deeper notch is likely to decrease the signal to noise ratio of the measurement. The more flexible beam element in the deeper notch is probably subjected to host of parasitic motions, all of which are detected by the strain gage. Table 6.3 compares the measurement quality of gages in the two different notches.

| | | Max error | Max abs error | Min abs error | Certainty (lbs) | % of full scale |
|---|---|---|---|---|---|---|
| Averages by notch | 1 | 5.38% | 32.19 | -25.52 | 57.72 | 2.89% |
| | 2 | 10.51% | 56.25 | -42.28 | 98.53 | 4.93% |

Table 6.3: Comparison of average errors and uncertainty for notches 1 and 2

It is interesting to note that the metal foil gage in notch two provides the most accurate measurements in all but two of the tests (1000 rpm 150 °F and 1200 rpm 150 °F). According to Table 6.3, however, of the two notch geometries tested, notch two is not the most accurate for preload measurement. Upon closer inspection, it was found that in each of the tests, the semiconductor gage in notch two was the most inaccurate of the four gages. This could have been a result of slight inconsistencies in the installation of the gage itself. Another potential cause of the inaccuracy of the semiconductor gage in notch two could be its high sensitivity. Because notch two contains a more flexible beam cross section, the semiconductor gage in this notch is able to measure strains exerted on the bearing cup that are not necessarily a result of applied preload. The high errors associated with this particular sensor and notch combination contributes to the high error averages for notch two.

Temperature and speed have no noticeable effect on gage measurement performance and repeatability. As long as the temperature and rotational speed of the bearing are both within the ranges tested here, there should not be a significant effect on the gage measurements.

Taking all of these factors into consideration, the optimal gage type to measure preload in a bearing is a metal foil gage. Not only does this gage provide optimal measurements, but also is also much easier to install and less sensitive to human errors that occur during installation. The high measurement sensitivity and accuracy of the semiconductor gage are offset by its mechanical fragility, and time consuming installation procedure resulting from this fragility. An optimal notch configuration cannot be accurately determined since only two notch geometries were compared. It suffices to say that the deeper notch (notch two) provides a more accurate sensor response.

## 6.3 Chapter Summary

The results of the experiments have been presented. In accordance with resistive strain gage theory, is has been assumed that the response of the gages should be linear. Gage performance has been quantified in terms of the linearity of the response, repeatability of the measurements, and deviation from the derived linear relation between bearing preload and notch strain. The metal foil gage in notch two has proven to be the most effective gage and notch geometry combination. Temperature and speed have no discernable effect on gage performance. In the

following chapter, conclusions will be drawn regarding the implications and applicability of this work, and suggestions will be made for further development of this measurement technique.

# Chapter 7   Conclusion and Recommendations

## 7.1   Thesis Conclusions

The significance of this work is in no way diminished because it was done with a single bearing geometry. An optimal gage type has been determined for this method of preload measurement. The signal-conditioning configuration has been designed for optimal performance for measurement of roller-induced strains. The gage installation and calibration procedure that has been described can easily be repeated for any bearing geometry. The goal of the calibration conducted was to demonstrate the repeatability of the gage measurement performance on an individual basis. The slight variations that existed between different gages were not extremely important in this case since, as has already been stated, a calibration would be necessary for each individual gage. The results of this effort are promising. The metal foil gage can provide preload measurements within 52 lbs of the actual applied preload, which is approximately 2.5% of the full scale tested. Optimal gage configuration would be determined based on the bearing size and geometry, and the desired measurement range.

## 7.2   Future Work

### 7.2.1   Bearing and System Analysis

As has already been mentioned, the finite element model that has been developed to simulate notch strains under bearing preload could be improved upon. In the current model, the roller-race contact was modeled as having an equal load distribution. In a tapered roller bearing, perfect line contact rarely exists. A more accurate model would take into account the multiple radii on the roller and undercuts in the cone, which both greatly affect the contact stresses on the rollers and therefore cup and cone. These improvements, in addition to those mentioned in section 7.1 could lead to a more accurate model.

The bearings that are used in automotive drive axles are pressed into a differential housing. In the work that has been conducted and previously presented in this paper, the differential housing was simulated as a simple rigid and symmetric structure both in the finite element model and experiments. In a real axle however, the housing is usually asymmetric and deforms under the axle loads. If the bearing cup is pressed into the differential housing with a tight fit, stresses in the differential are passed onto the bearing cup. These housing stresses induce strains on the cup outer diameter. If a strain gage is located in the vicinity of these housing stress concentrations, it could measure parasitic strains resulting not from bearing preload, but from these housing stresses. A detailed finite element model of the differential housing would be necessary to determine the optimal angular position of the strain gages on the bearing cup with respect to the differential housing.

### 7.2.2   Active Preload Control

A logical development stemming from this preload sensing bearing would be a closed loop preload control mechanism; applications in several industries could greatly benefit from such development. Preload has a direct and significant impact on bearing life. Since optimal preloads are known for various operating conditions in different systems, an actuation device could be paired with this preload measurement technique to create a closed-loop bearing preload control

system. Piezoelectric ceramic rings could be used as the actuator in such a system. An actuator of this type seems most appropriate because of its size, and symmetry with the existing geometry of the bearing and related components. Piezoelectric devices have been previously used as noise canceling devices; this strategy could be employed in a preload control system by operating the feedback control loop at high frequencies.

# Appendix A

The following equations describe how strain measurements are obtained from resistance changes in the gage. Amplifier gains and excitation currents were selected based upon the desire to obtain voltage outputs of 0 to 10 V. This output range was optimal for the specific amplifiers and signal conditioners used in the experiments.

$$dR = \varepsilon * R_{gage} * GF$$

$$V_{IN} = dR * I_{excitation}$$
$$V_{IN} = \varepsilon * R_{gage} * GF * I_{excitation}$$

$$V_{OUT} = Gain\left(\varepsilon * R_{gage} * GF * I_{excitation}\right)$$

$$Gain = V_{OUT} / V_{IN}$$

## Appendix B

Torque Test machine.



Lubricating oil

Strain gage wire leads
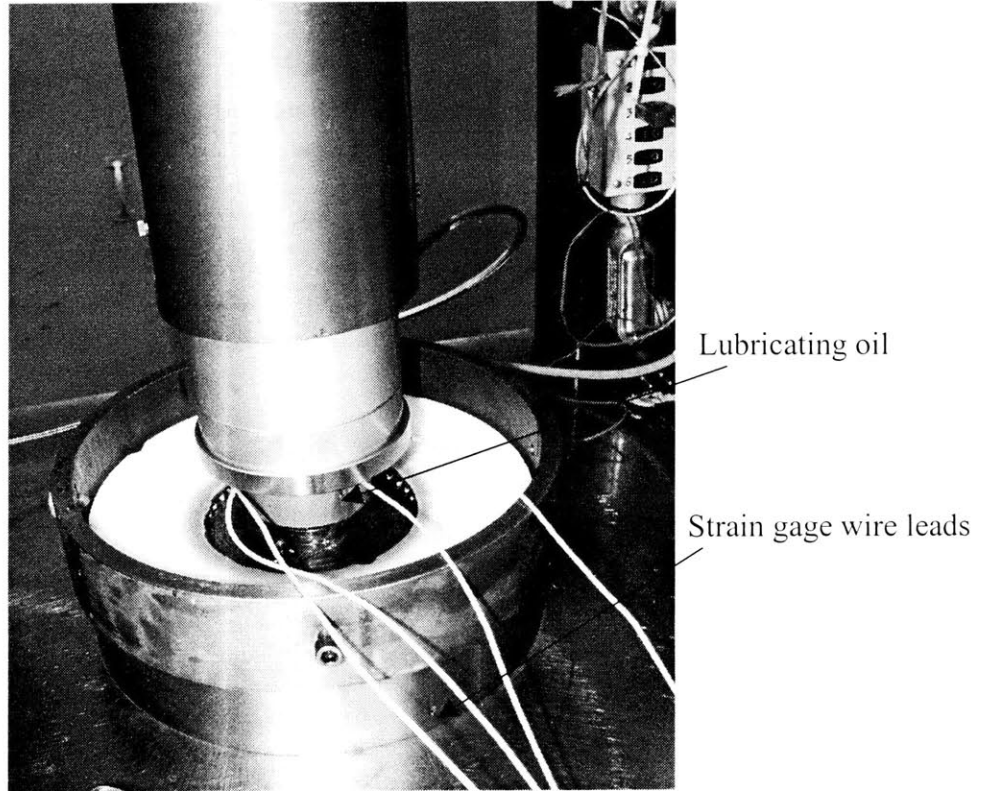
Control unit for the Torque Test Machine.



Input rotational
speed (rpm)

Input axial load
(lbs)

Data acquisition
software running
on laptop
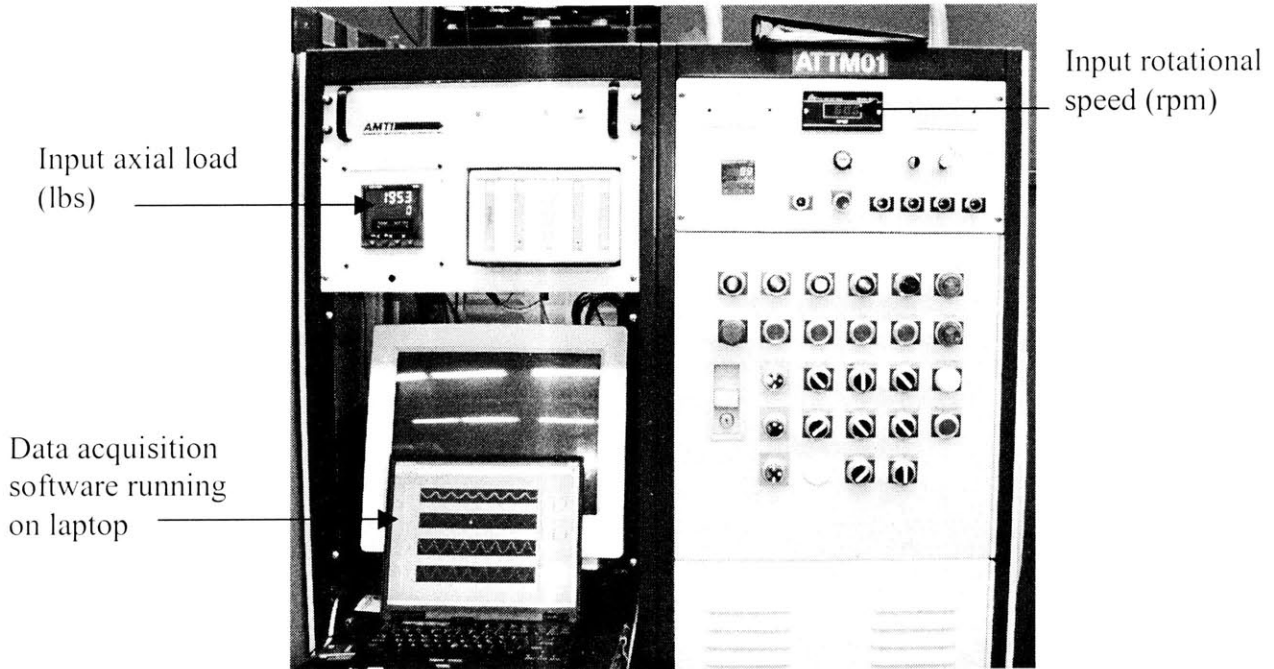
## Appendix C

The following plots show the difference in gage response for the two different gage types. The strain measured by the metal foil gage is consistently approximately twice that of the strain measured by the semiconductor gage, regardless of speed or temperature. The first plot shows that this relationship is consistent regardless of temperature (compare with Figure 6.1). The second plot shows that this behavior is consistent regardless of speed.





40
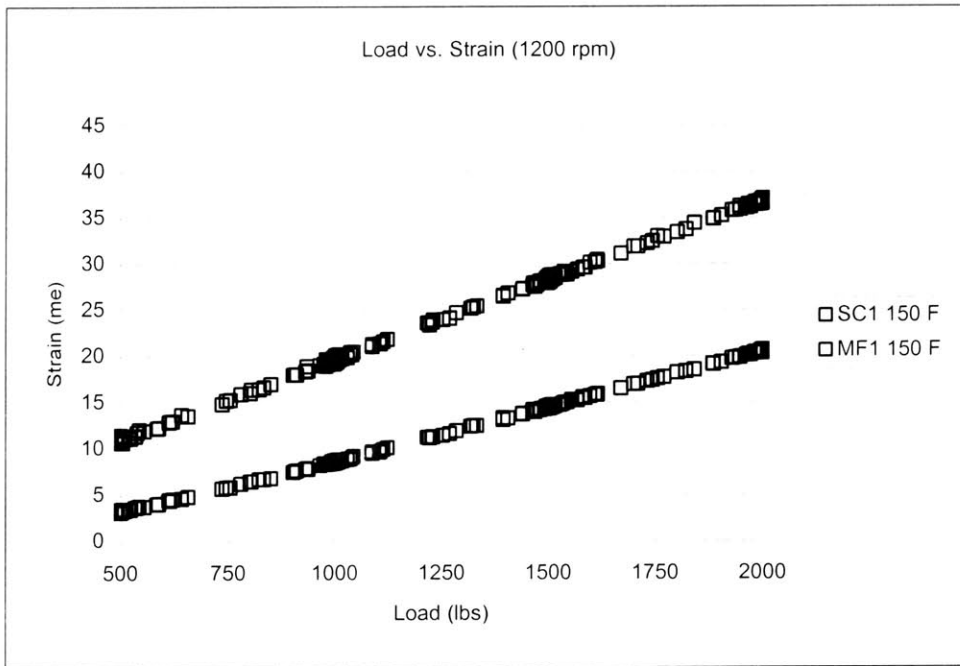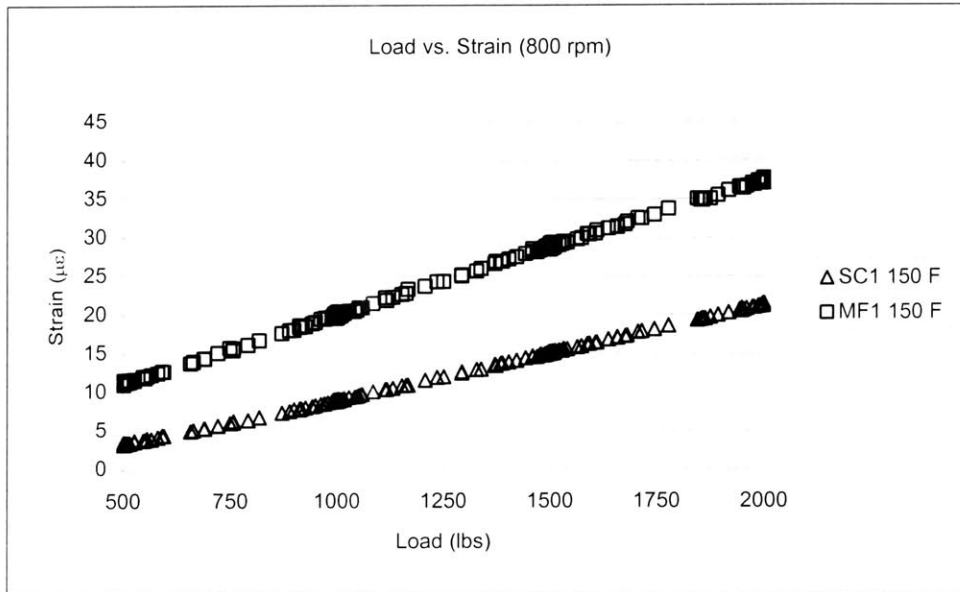
The following tables illustrate the consistency of the results regardless of rotational speed. Note the repeatability of the slopes of each of the linear fits. The first table summarizes the data for 100 °F, and the second for 150 °F.

| | | Max error | Certainty (lbs) | error % of full scale | Avg Temp (F) | y=mx+b | |
| --- | --- | --- | --- | --- | --- | --- | --- |
| | | | | | | m | b |
| | 800 rpm | 4.69% | 51.57 | 2.58% | 99.7 | 0.0121 | -2.8229 |
| SC1 100 F | 1000 rpm | 6.51% | 64.48 | 3.17% | 99.8 | 0.012 | -2.4907 |
| | 1200 rpm | 6.95% | 57.16 | 2.86% | 101.1 | 0.0119 | -2.7831 |
| | | | | | | | |
| | 800 rpm | 15.03% | 138.69 | 6.93% | 103.6 | 0.0176 | 2.6099 |
| SC2 100 F | 1000 rpm | 15.76% | 144.75 | 7.24% | 103.6 | 0.0175 | 3.0219 |
| | 1200 rpm | 13.48% | 129.7 | 6.49% | 105.5 | 0.0177 | 2.5129 |
| | | | | | | | |
| | 800 rpm | 2.83% | 47.06 | 2.35% | 102.7 | 0.0176 | 2.6099 |
| MF1 100 F | 1000 rpm | 5.06% | 64.04 | 3.20% | 102.8 | 0.0175 | 3.0219 |
| | 1200 rpm | 5.68% | 73.96 | 3.70% | 104.8 | 0.0177 | 2.5129 |
| | | | | | | | |
| | 800 rpm | 3.51% | 32.01 | 1.60% | 104.8 | 0.0231 | -2.4063 |
| MF2 100 F | 1000 rpm | 6.94% | 58.72 | 2.94% | 105 | 0.0231 | -1.913 |
| | 1200 rpm | 5.91% | 57.1 | 2.85% | 107 | 0.0233 | -2.3 |

| | | Max error | Certainty (lbs) | error % of full scale | Avg Temp (F) | y=mx+b | |
| --- | --- | --- | --- | --- | --- | --- | --- |
| | | | | | | m | b |
| | 800 rpm | 7.13% | 56.63 | 2.83% | 143.6 | 0.012 | -2.9447 |
| SC1 150 F | 1000 rpm | 5.55% | 55.38 | 2.77% | 144 | 0.0119 | -3.0264 |
| | 1200 rpm | 6.78% | 67.8 | 3.39% | 144.6 | 0.0116 | -2.792 |
| | | | | | | | |
| | 800 rpm | 16.28% | 155.46 | 7.77% | 147.8 | 0.0127 | -4.1742 |
| SC2 150 F | 1000 rpm | 15.73% | 152.92 | 7.65% | 148.2 | 0.0125 | -4.1454 |
| | 1200 rpm | 16.58% | 153.64 | 7.68% | 148.7 | 0.0121 | -3.7058 |
| | | | | | | | |
| | 800 rpm | 3.67% | 53.41 | 2.67% | 146.8 | 0.0175 | 2.4202 |
| MF1 150 F | 1000 rpm | 3.80% | 49.32 | 2.47% | 147.3 | 0.0175 | 2.2525 |
| | 1200 rpm | 5.98% | 52.79 | 2.64% | 147.8 | 0.0173 | 2.282 |
| | | | | | | | |
| | 800 rpm | 4.39% | 49.57 | 2.48% | 148.9 | 0.0233 | -3.1652 |
| MF2 150 F | 1000 rpm | 5.80% | 51.36 | 2.57% | 149.3 | 0.0233 | -3.3445 |
| | 1200 rpm | 6.66% | 58.47 | 2.92% | 150 | 0.0229 | -3.1351 |

The following tables show the stability and repeatability of the gage response for two temperatures: 100 °F and 150 °F.

| | | | | | | y=mx+b | |
|---|---|---|---|---|---|---|---|
| | | Max error | Certainty (lbs) | error % of full scale | Avg Temp (F) | m | b |
| SC1 800 rpm | 100 F | 4.69% | 51.57 | 2.85% | 99.7 | 0.0121 | -2.8229 |
| | 150 F | 7.13% | 56.63 | 2.83% | 143.6 | 0.012 | -2.9447 |
| | | | | | | | |
| SC2 800 rpm | 100 F | 15.03% | 138.69 | 6.93% | 103.6 | 0.0127 | -3.734 |
| | 150 F | 16.28% | 155.46 | 7.77% | 147.8 | 0.0127 | -4.1742 |
| | | | | | | | |
| MF1 800 rpm | 100 F | 2.83% | 47.06 | 2.35% | 102.7 | 0.0176 | 2.6099 |
| | 150 F | 3.67% | 53.41 | 2.67% | 146.8 | 0.0175 | 2.4202 |
| | | | | | | | |
| MF2 800 rpm | 100 F | 3.51% | 32.01 | 1.60% | 104.8 | 0.0231 | -2.4063 |
| | 150 F | 4.39% | 49.57 | 2.48% | 148.9 | 0.0233 | -3.1652 |

| | | | | | | y=mx+b | |
|---|---|---|---|---|---|---|---|
| | | Max error | Certainty (lbs) | error % of full scale | Avg Temp (F) | m | b |
| SC1 1000 rpm | 100 F | 6.51% | 63.48 | 3.17% | 99.8 | 0.012 | -2.4907 |
| | 150 F | 5.55% | 53.38 | 2.77% | 144 | 0.0119 | -3.0204 |
| | | | | | | | |
| SC2 1000 rpm | 100 F | 15.76% | 144.75 | 7.24% | 103.6 | 0.0128 | -3.6596 |
| | 150 F | 15.73% | 152.92 | 7.65% | 148.2 | 0.0125 | -4.1454 |
| | | | | | | | |
| MF1 1000 rpm | 100 F | 5.06% | 64.04 | 3.20% | 102.8 | 0.0175 | 3.0219 |
| | 150 F | 3.80% | 49.32 | 2.47% | 147.3 | 0.0175 | 2.2525 |
| | | | | | | | |
| MF2 1000 rpm | 100 F | 6.94% | 58.72 | 2.94% | 105 | 0.0231 | -1.913 |
| | 150 F | 5.80% | 51.36 | 2.57% | 149.3 | 0.0233 | -3.3445 |

|  |  | Max error | Certainty (lbs) | error % of full scale | Avg Temp (F) | y=mx+b | |
|---|---|---|---|---|---|---|---|
|  |  |  |  |  |  | m | b |
| SC1 1200 rpm | 100 F | 6.95% | 57.16 | 2.86% | 101.7 | 0.0119 | -2.7831 |
|  | 150 F | 6.78% | 67.8 | 3.39% | 144.6 | 0.0116 | -2.792 |
|  |  |  |  |  |  |  |  |
| SC2 1200 rpm | 100 F | 13.48% | 129.7 | 6.49% | 105.5 | 0.0126 | -3.5151 |
|  | 150 F | 16.58% | 153.64 | 7.68% | 148.7 | 0.0121 | -3.7058 |
|  |  |  |  |  |  |  |  |
| MF1 1200 rpm | 100 F | 5.68% | 73.96 | 3.70% | 104.8 | 0.0177 | 2.5129 |
|  | 150 F | 5.98% | 52.79 | 2.64% | 147.8 | 0.0173 | 2.289 |
|  |  |  |  |  |  |  |  |
| MF2 1200 rpm | 100 F | 5.91% | 57.1 | 2.85% | 107 | 0.0233 | -2.3 |
|  | 150 F | 6.66% | 58.47 | 2.92% | 150 | 0.0229 | -3.1351 |

# Bibliography

"Battle Against Friction: The History & Development of Anti-Friction Bearings." Canton, OH: The Timken Company, 1994.

"Bearing setting techniques." Canton, OH: The Timken Company, 1985.

Coffey, Keith, and Johnston, Jerome. "Getting The Most Out of Strain Gauge Load Cells." Sensors (2000): 52-61.

Garcia-Bonito J, Brennan M J, Elliot S J, David A, and Pinnington R J. "A novel high-displacement piezoelectric actuator for active vibration control." Smart Materials and Structures 7 (1998): 31-42.

Hearn, Edwin J. Strain Gauges. Watford Herts, England: Merrow Publishing Co. Ltd, 1971.

Joki, Mark A., and Lindsay, Kenneth W. System for Monitoring the Operating Conditions of a Bearing. The Timken Company. Patent 6,490,935 Dec. 10 2002.

Leibensperger, Robert L. "So You Think You Know All About Bearing Preload." Machine Design 40 (1972).

Lissner, H. R., Perry, C. C. The Strain Gage Primer. New York: McGraw-Hill, 1955.

Martin, Berthold, and Hill, Harold E. "Design and Selection Factors for Automatic Transaxle Tapered Roller Bearings." Symposium. SAE Technical Paper Series. Detroit, Michigan: SAE, 1992.

Moseley, John and McLarty, Daniel. Bearing With Adjustable Stiffness. The Torrington Company. Patent 4,850,719 Jul. 25 1989.

Ott, Lyman. An Introduction to Statistical Methods and Data Analysis. Belmont, California: Wadsworth Publishing Company, Inc., 1977.

Pallás-Areny, Ramón, and Webster, John G. Sensors and Signal Conditioning. New York: John Wiley & Sons, Inc., 1991.

Slocum, Alex. Precision Machine Design. Dearborn: Society of Mechanical Engineers, 1992.

Tang P, Palazzo A, Kascak A, Montagne G, and Li W. "Combined piezoelectric-hydraulic actuator based active vibration control for rotordynamic systems." Journal of Vibration and Acoustics Transactions ASME 117 (1995): 285-93.